View Online / Journal Homepage
Dynamic Article Links

Energy & Environmental Science

Cite this: DOI: 10.1039/c2ee02818b

www.rsc.org/ees

PAPER

High pressure driven structural and electrochemical modifications in layered lithium transition metal intercalation oxides†

C. R. Fell,[a] D. H. Lee,[b] Y. S. Meng,*[ab] J. M. Gallardo-Amores,[c] E. Morán[c] and M. E. Arroyo-de Dompablo*[d]

Received 3rd October 2011, Accepted 15th December 2011
DOI: 10.1039/c2ee02818b

Downloaded by University of California - San Diego on 01 February 2012
Published on 01 February 2012 on http://pubs.rsc.org | doi:10.1039/C2EE02818B

High pressure–high temperature (HP/HT) methods are utilized to introduce structural modifications in the layered lithium transition metal oxides $LiCoO_2$ and $Li[Ni_xLi_{1/3-2x/3}Mn_{2/3-x/3}]O_2$ where $x = 0.25$ and 0.5. The electrochemical property to structure relationship is investigated combining computational and experimental methods. Both methods agree that the substitution of transition metal ions with Li ions in the layered structure affects the compressibility of the materials. We have identified that following high pressure and high temperature treatment up to 8.0 GPa, $LiCoO_2$ did not show drastic structural changes, and accordingly the electrochemical properties of the high pressure treated $LiCoO_2$ remain almost identical to the pristine sample. The high pressure treatment of $LiNi_{0.5}Mn_{0.5}O_2$ ($x = 0.5$) caused structural modifications that decreased the layered characteristics of the material inhibiting its electrochemical lithium intercalation. For $Li[Li_{1/6}Ni_{1/4}Mn_{7/12}]O_2$ more drastic structural modifications are observed following high pressure treatment, including the formation of a second layered phase with increased Li/Ni mixing and a contracted *c*/*a* lattice parameter ratio. The post-treated $Li[Li_{1/6}Ni_{1/4}Mn_{7/12}]O_2$ samples display a good electrochemical response, with clear differences compared to the pristine material in the 4.5 voltage region. Pristine and post-treated $Li[Li_{1/6}Ni_{1/4}Mn_{7/12}]O_2$ deliver capacities upon cycling near 200 mA h g^{-1}, even though additional structural modifications are observed in the post-treated material following electrochemical cycling. The results presented underline the flexibility of the structure of $Li[Li_{1/6}Ni_{1/4}Mn_{7/12}]O_2$; a material able to undergo large structural variations without significant negative impacts on the electrochemical performance as seen in $LiNi_{0.5}Mn_{0.5}O_2$. In that sense, the Li excess materials are superior to $LiNi_{0.5}Mn_{0.5}O_2$, whose electrochemical characteristics are very sensitive to structural modifications.

[a] *Department of Materials Science and Engineering, University of Florida, Gainesville, FL, 32611, USA*
[b] *Department of NanoEngineering, University of California San Diego, La Jolla, CA, 92037, USA. E-mail: shirleymeng@ucsd.edu*
[c] *Laboratorio de Altas Presiones, Facultad de Ciencias Químicas, Universidad Complutense de Madrid, 28040 Madrid, Spain*
[d] *Malta-Consolioder Team, Facultad de Ciencias Químicas, Universidad Complutense de Madrid, 28040 Madrid, Spain. E-mail: e.arroyo@quim.ucm.es*

† Electronic supplementary information (ESI) available. See DOI: 10.1039/c2ee02818b

Broader context

Rechargeable lithium ion batteries are key components of portable electronics and play an important role in today's mobile society. To expand their applications into onboard energy storage for electric vehicles, the energy density and cycle-life must be increased in meeting the new demands. Layered oxide positive electrode materials that can be charged to higher potentials (more than 4 V) with higher specific capacities provide a possible solution. It is well known that the synthesis conditions play a critical role in determining the microstructure, morphology and surface characteristics, thereby influencing the electrochemical response. In this work, we have induced structural modifications in $LiCoO_2$ and $Li[Ni_xLi_{1/3-2x/3}Mn_{2/3-x/3}]O_2$ ($x = 1/4$ and 1/2) using high pressure–high temperature treatment in order to obtain a better understanding of the electrochemical dependence on structural factors. Surprisingly the layered "lithium excess" material shows the ability to undergo large compressions and structural modifications while delivering good electrochemical capacities. Our research findings provide significant new insights into understanding the complex relationship of crystal structure and electrochemical performance in layered oxides.

Downloaded by University of California - San Diego on 01 February 2012
Published on 01 February 2012 on http://pubs.rsc.org | doi:10.1039/C2EE02818B

1. Introduction

Rechargeable lithium ion batteries are key components of portable electronics and play an important role in today's mobile society. To expand the use of lithium ion batteries, for instance as the onboard energy storage for vehicles, the energy density must be increased. Layered oxide positive electrode materials that can be charged to higher potentials (more than 4 V) with higher specific capacities provide a possible solution. Two widely studied layered oxide positive electrode materials are $LiCoO_2$ and $Li[Ni_xLi_{1/3-2x/3}Mn_{2/3-x/3}]O_2$. The crystal structure of the Li-excess material is shown in Fig. 1. $LiCoO_2$ has been commercialized for two decades. The crystal structure is composed of alternating layers of lithium and cobalt ions in a close packed oxygen array. The lithium ions are reversibly intercalated between the transition metal–oxygen (MO) layers. Replacing Co by Ni and Mn leads to $LiNi_{0.5}Mn_{0.5}O_2$, a typical multi-electron redox system showing a synergetic combination of Mn^{4+} and Ni^{2+}. In this material, Mn^{4+} remains unchanged and stabilizes the structure when Li is extracted. Ni^{2+} can be fully oxidized to Ni^{4+}, thereby compensating the fact that Mn^{4+} cannot be oxidized.[1,2] This material delivers 200 mA h g^{-1} reversible capacity between 3 and 4.5 V.[3] The layered "lithium excess" transition metal oxides, $Li[Ni_xLi_{1/3-2x/3}Mn_{2/3-x/3}]O_2$ ($0 < x < 1/2$), are of great interest as a new generation of positive electrode materials since they deliver higher reversible capacity exceeding 250 mA h g^{-1} at a lower cost compared with both $LiCoO_2$ and $LiNi_{0.5}Mn_{0.5}O_2$. In these materials the excess lithium is positioned in the transition metal layer inducing cation ordering[4] (see Fig. 1b). Moreover, there is a partial mixing of Li and Ni up to 15% between the layers due to the similarities in ionic radii.[5] During the initial charging region, the capacity originates from the oxidation of Ni^{2+} to Ni^{4+} up to 4.4 V. At 4.45 V, a high voltage plateau region appears associated with an irreversible capacity of 50 to 100 mA h g^{-1}. The anomalous high capacities have been attributed to an irreversible loss of oxygen from the lattice during the first charge accompanied by Li removal and/or surface reaction through electrode/electrolyte reduction.[6–11] Though a clear explanation of the source of the additional capacity is still under debate, previous work has consistently shown changes in the cation arrangement and crystal structure upon electrochemical cycling to 4.8 V. Previous research has identified the disappearance of the cation ordering in the transition metal layer following electrochemical cycling.[7,12] Our previous research has also observed the expansion of the *c*/*a* lattice ratio and increased Li/Ni interlayer mixing following ten electrochemical cycles.[12] Moreover, during electrochemical cycling the material undergoes large changes in lattice parameters as well as increases in strain.[8] However, the material is able to reversibly cycle with large capacities and little capacity fade although undergoing serious structural modifications during the first electrochemical cycle.

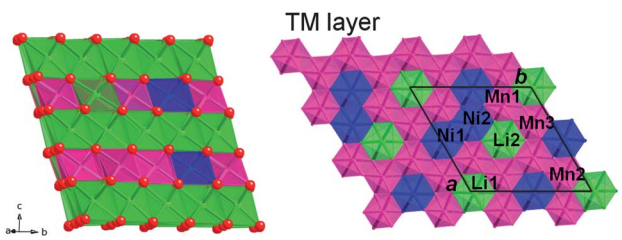

Fig. 1 Crystal structure of the layered oxides under investigation showing the ordering in the Li excess material $Li[Li_{1/6}Ni_{1/4}Mn_{7/12}]O_2$. A view of the TM layer is shown in the right panel (b). Color code: Li green, Mn pink, Ni blue and O red.

For the $Li[Ni_xLi_{1/3-2x/3}Mn_{2/3-x/3}]O_2$ ($0 < x < 0.5$) family it is well documented that the synthesis conditions play a critical role in determining the microstructure, morphology and surface characteristics, thereby influencing the electrochemical response. Our recent investigation on uncoated pristine $Li[Li_{1/3-2x/3}Ni_xMn_{2/3-x/3}]O_2$ revealed that the reversible discharge capacity was affected by the synthesis conditions.[12] The first cycle irreversible capacity could be significantly reduced by controlling the precursor chemistry to prevent the formation of the surface –OH group. Efforts to achieve a better understanding of the electrochemistry of Li-excess materials involve the connection of crystal structure to electrochemical properties. High pressure–high temperature (HP/HT) techniques are a useful tool to induce structural modifications of materials. It has been previously reported that treatment of complex ceramic materials under increased pressures results in cation arrangements that are not typically possible at atmospheric pressure.[13–15] The high pressure treatment changes both the crystal structure as well as the electronic characteristics of the material. High pressure driven transformations of several electrode materials have been studied and reported, for example, Li_xMPO_4 (M=Fe and Co),[14,16] V_2O_5,[17] Ga doped-$LiNiO_2$,[18] and $Li[Li_xNi_{1-x}]O_2$.[19] It is proven that after exposure to high pressure/high temperature conditions, the electrochemical properties varied compared to the ambient pressure materials.

So far little is known about the effect of high pressure on the structure of the layered $LiMO_2$ materials. Work by Wang *et al.* compared experimental (*in situ*) high pressure structural and vibrational properties to *ab initio* calculations for $LiCoO_2$. They found that the structure remains layered up to at least 26 GPa at room temperature,[20] though an important compression of the structure is observed (the *c*/*a* ratio decreases about 5%). The electrochemistry of the post-treated materials was not explored. Recent work focused on the synthesis of $Li_{1+x}(Ni_{1/2}Mn_{1/2})_{1-x}O_2$ ($x = 0$ and 0.2) under uniaxial pressure.[21] In this approach a mixture of reactants is subjected to high pressure/high temperature conditions. The authors found that the increased pressure of synthesis created different cation distributions and varying oxidation states in the Ni ions. The high pressure synthesis resulted in a mixture of phases displaying poor reversible electrochemical properties compared to pristine materials.

The aim of this research is to investigate the effect of HP/HT treatment on the structure and electrochemical properties of $Li[Ni_xLi_{1/3-2x/3}Mn_{2/3-x/3}]O_2$ where $x = 0.25$ and 0.5 (*i.e.* $Li[Li_{1/6}Ni_{1/4}Mn_{7/12}]O_2$ and $LiNi_{0.5}Mn_{0.5}O_2$) in comparison to those of $LiCoO_2$. With this objective, we have combined HP/HT synthesis techniques, X-ray diffraction, electrochemical testing and first principles computation with Density Functional Theory (DFT). We will show how the structural modifications introduced by the HP/HT treatment influence the electrochemical response of the layered materials to demonstrate the superior ability of the Li excess materials to accommodate structural modifications while retaining excellent electrode characteristics.

 This journal is © The Royal Society of Chemistry 2012

Downloaded by University of California - San Diego on 01 February 2012
Published on 01 February 2012 on http://pubs.rsc.org | doi:10.1039/C2EE02818B

2. Methodologies

2.1 Computational

Total energies of the lithium excess material $Li[Li_{0.16}Ni_{0.25}Mn_{0.583}]O_2$ (or $Li[Li_{1/6}Ni_{1/4}Mn_{7/12}]O_2$) and stoichiometric $LiNi_{0.5}Mn_{0.5}O_2$ were calculated within the DFT + U framework as implemented in the VASP package.[22–24] In the simulated cell of $LiNi_{0.5}Mn_{0.5}O_2$ the Mn and Ni ions are arranged in a zigzag manner. This Ni–Mn ordering is almost degenerate in energy with the most likely flower-like pattern,[25] and it was chosen for simplicity in this work. In the cell considered for $Li[Li_{1/6}Ni_{1/4}Mn_{7/12}]O_2$, there are four layers: two oxygen layers, one transition metal (TM) layer and one Li layer (48 atoms). Each layer is composed of twelve ions, forming an in-plane supercell $\sqrt[2]{3a_{hex.}} \times \sqrt[2]{3a_{hex.}}$. Oxygen ions are close-packed and stacked in ABC (O3) stacking, serving as the frame, while the TM slab and Li slab stack alternatively. To simulate the $Li[Li_{1/6}Ni_{1/4}Mn_{7/12}]O_2$ material a complex ordering has to be imposed on the TM layer. In a recent work, it was found that in the most stable configuration the two "excess" Li ions located in the TM layer have distinct environments; one Li ion is surrounded by 6 Mn ions and the other Li ion is surrounded by 5 Mn ions plus 1 Ni ion (see Fig. 1b). Such ordering is compatible with experimental observations. A detailed description of this crystal model is given in ref. 26.

As a first step, the structures were fully relaxed (cell parameters, volume and atomic positions) and the final energies of the optimized geometries were recalculated so as to correct the changes in the basis set of the wave functions during relaxation. Computational details are given in our previous works.[26] Secondly, the relaxed structure calculations within the GGA + U approximation were performed at various constant volumes and the energy–volume data were fitted to the Murnaghan equation of state.[27]

Lithium mobility in delithiated $Li[Li_{1/6}Ni_{1/4}Mn_{7/12}]O_2$ at ambient pressure and at 8 GPa was investigated using the Nudged Elastic Band (NEB) method as implemented in VASP. The energetic path for Li motion from one octahedral to adjacent octahedral site across a tetrahedral site in the Li layer was studied at the concentration $Li_{5/6}[Li_{1/6}Ni_{1/4}Mn_{7/12}]O_2$. Constant volume calculations were performed for three intermediate images not further apart than 0.8 Å. To preserve pressure the volume was fixed at that of the lithiated phases. To calculate the energy at the saddle point, cubic splines were fit through the images along each hop.

2.2 Experimental

2.2.1 Synthesis. Lithium cobalt oxide (Sigma Aldrich) powders were used as obtained. The lithium excess materials $Li[Ni_xLi_{1/3-2x/3}Mn_{2/3-x/3}]O_2$ where $x = 0.25$ and 0.5 were synthesized using the coprecipitation technique previously described.[12] Transition metal nitrates, $Ni(NO_3)_2 \cdot 6H_2O$ (Fisher) and $Mn(NO_3)_2 \cdot 4H_2O$ (Fisher), were titrated into a stoichiometric $LiOH \cdot H_2O$ solution for a duration of two hours. The co-precipitated transition metal hydroxides were then filtered using a vacuum filter and washed three times with deionized water. The collected transition metal hydroxides were dried in an oven at 180 °C for 10 hours in air. The dried transition metal precursors were mixed with a stoichiometric amount of $LiOH \cdot H_2O$ corresponding to the amount of $M(OH)_2$ from the coprecipitation step. This mixture was ground for 30 minutes to ensure adequate mixing and then placed in a furnace at 480 °C for 12 hours. The precalcinated powders were prepared as a pellet for high temperature sintering. These samples were then calcinated at 1000 °C for 12 hours in air. Samples were brought back to room temperature by furnace cooling.

2.2.2 High pressure–high temperature treatment. Following the ambient pressure synthesis, $LiCoO_2$, $LiNi_{0.5}Mn_{0.5}O_2$ and $Li[Li_{1/6}Ni_{1/4}Mn_{7/12}]O_2$ were subjected to HP/HT treatment using different presses: Belt or Conac types for hydrostatic pressure up to 8 GPa, and Rockland for uniaxial pressure up to 3 GPa. No differences were observed whether uniaxial or hydrostatic pressure is applied. Samples were exposed to HP/HT treatment with pressures in the range of 3.0–8.0 GPa and temperatures between 800 and 1000 °C. After applying the pressure and temperature for one hour, the anvil is quenched to room temperature while pressure is slowly released.

2.2.3 Structural characterization. Powder X-ray diffraction patterns were taken on a Siemens D-5000 and X'Pert Pro Alpha I laboratory X-ray diffractometers. Powder diffractions of as-synthesized $Li[Li_{1/6}Ni_{1/4}Mn_{7/12}]O_2$ and $Li[Li_{1/6}Ni_{1/4}Mn_{7/12}]O_2$ following high pressure/high temperature treatment at 5.2 GPa were taken using synchrotron X-ray diffraction at the Advanced Photon Source (APS) at Argonne National Laboratory (ANL) on a beamline 11-BM ($\lambda = 0.4122$ Å). Synchrotron X-ray diffraction patterns of electrochemically cycled $Li[Li_{1/6}Ni_{1/4}Mn_{7/12}]O_2$ following high pressure treatment were also collected by the beamline 11-BM. The cycled samples were hermetically sealed in 0.8 mm Kapton capillaries to minimize air-exposure.

2.2.4 Electrochemistry. Electrochemical properties were measured on an Arbin battery cycler in galvanostatic mode. Cathodes were prepared by mixing the active material ($LiCoO_2$ or $Li[Ni_xLi_{1/3-2x/3}Mn_{2/3-x/3}]O_2$) with 10 wt% Super P carbon (TIMCAL) and 10 wt% polyvinylidene fluoride (PVDF) in *N*-methylpyrrolidone (NMP) solution. The slurry was cast onto Al foil using a doctor blade and dried in a vacuum oven at 80 °C. The electrode discs were punched and dried again at 80 °C for 6 h before storing them in an argon filled glove box (H_2O level < 1 ppm). The active material loading of the cathode disks is approximately 5–10 mg cm^{-2}. 2016 type coin cells and Swagelok cells were used to study the electrochemical behavior of the compounds and cycled samples for XRD. The batteries were prepared in an Argon glove box using a lithium metal ribbon anode and 1 M $LiPF_6$ in a 1 : 1 ethylene carbonate : dimethyl carbonate (EC : DMC) electrolyte solution (Novolyte). A Celgard model C480 separator (Celgard Inc., USA) was used as the separator.

The cycled samples for XRD were recovered by disassembling cycled batteries in an argon-filled glove box. The cathode was washed by submerging in acetonitrile (H_2O < 10 ppm) 3 times. The cathode was allowed to dry in argon atmosphere overnight. The powder was scraped and mounted in a hermetically sealed capillary for *ex situ* X-ray diffraction.

Downloaded by University of California - San Diego on 01 February 2012
Published on 01 February 2012 on http://pubs.rsc.org | doi:10.1039/C2EE02818B

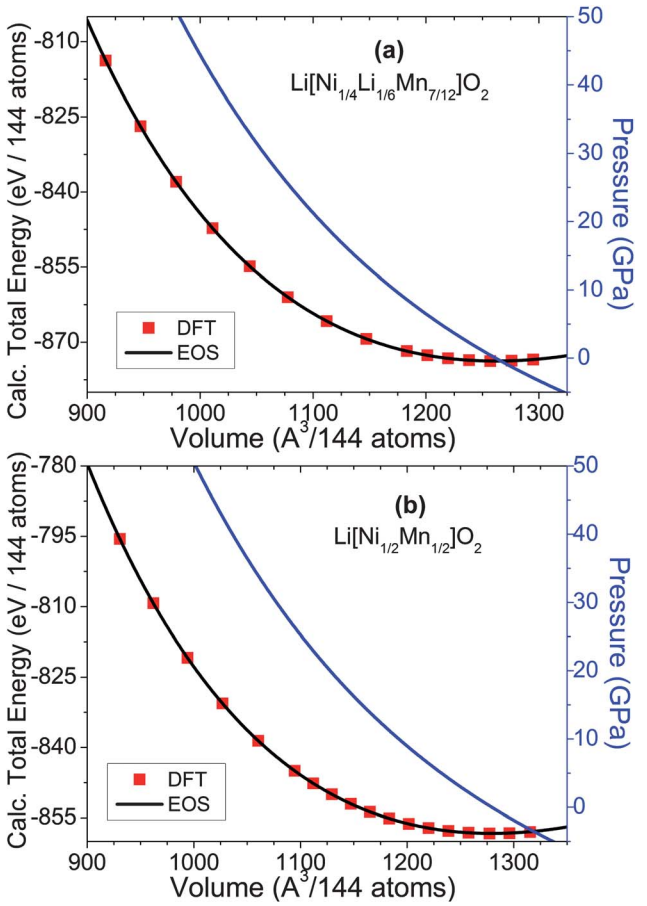

Fig. 2 Calculated total energy as a function of the volume for $Li[Li_{1/6}Ni_{1/4}Mn_{7/12}]O_2$ (a) and $LiNi_{0.5}Mn_{0.5}O_2$ (b). Symbols correspond to the DFT data and the black line shows the fit to the Murnaghan equation of states. The dependence of pressure with volume is given in the right axis.

3. Results

3.1 Computational

DFT methods are a powerful tool to evaluate materials behavior under high pressure. Fig. 2 shows the calculated total energy as a function of the volume for $Li[Li_{1/6}Ni_{1/4}Mn_{7/12}]O_2$ (Fig. 2a) and $LiNi_{0.5}Mn_{0.5}O_2$ (Fig. 2b), together with the corresponding fit of the DFT data to the Murnaghan equation of state (EOS).[27] From the fitting to the EOS, one can extract the variation of pressure as a function of the volume (right axis in Fig. 2). Note that the volume corresponds to 144 atoms to facilitate comparison with experiments. Table 1 compares the parameters of the DFT data fitted to the EOS, with those experimentally and computationally obtained for $LiCoO_2$. $LiNi_{0.5}Mn_{0.5}O_2$ and $Li[Li_{1/6}Ni_{1/4}Mn_{7/12}]O_2$ exhibit bulk moduli of 125 GPa and 117 GPa, respectively. These values are lower than the bulk modulus found for $LiCoO_2$ (149 GPa), suggesting that Ni and Mn substitution for Co in the TM layer produces a softer, more compressible material. The Li-excess material is more compressible than the stoichiometric $LiNi_{0.5}Mn_{0.5}O_2$ due to the presence of Li ions in the TM layer, as discussed below.

Table 1 Calculated equation of state parameters for layered-Li $[Li_xM_{1-x}]O_2$ materials. E_0, V_0, B_0 and B_0' are the zero-pressure energy, volume, bulk modulus and its pressure derivative, respectively. Experimental values are given in parentheses

Compound	B_0/Gpa	B_0'	V_0/A^3	E_0/eV
$LiCoO_2$[20]	142 (149)	4.51 (4.1)	1186.06 (1157)	
$LiNi_{0.5}Mn_{0.5}O_2$	125	3.8	1278.70 (1241)	−858.24
$Li[Li_{1/6}Ni_{1/4}Mn_{7/12}]O_2$	117	3.9	1261.58 (1219)	−873.76

Fig. 3 shows the calculated Li–O and M–O bond lengths as a function of volume for $Li[Li_{1/6}Ni_{1/4}Mn_{7/12}]O_2$, up to a pressure of 19 GPa (for volume–pressure dependence with volume see Fig. 2). The cationic ordering in the TM layers is depicted in the right side of Fig. 1b. The Li–O bonds compress 5.8% in the Li layer and 4.4% or 2.4% depending on the local environment in the TM layer. The Mn–O and Ni–O bonds are more difficult to compress than Li–O with their relative compressibility being 2.4% and 3%, respectively. The larger Ni cation renders a more compressible Ni–O bond. The predicted bond compressibility is similar to those found in $LiCoO_2$:[20] Li–O 5.2% and Co–O 1.5%. The Li–O bonds, in the Li layer, are about two to three times more compressible than the M–O bonds in the TM layer. It is plausible that the lower bulk moduli of $Li[Li_{1/6}Ni_{1/4}Mn_{7/12}]O_2$ compared to $LiNi_{0.5}Mn_{0.5}O_2$ are due to a more compressible TM layer on account of the presence of Li ions.

The compression of these layered materials is anisotropic. Experimental results for $LiCoO_2$ show evidence of 1.5% and 2.8% contraction for the *a* and *c* lattice parameters, respectively, between ambient pressure and 19.9 GPa. The calculated data yield compressions of 3.5% (*a* parameter) and 5% (*c* parameter) for $Li[Li_{1/6}Ni_{1/4}Mn_{7/12}]O_2$ in the same pressure range. The anisotropic compression of the structure is correlated to the different compressions of inter-plane and in-plane bonds. Fig. 4 shows the calculated in-plane and inter-plane contractions between adjacent metal ions for $Li[Li_{1/6}Ni_{1/4}Mn_{7/12}]O_2$. The inter-plane distances are shortened more than in-plane distances independent of the ion (Li, Mn, or Ni), in good agreement with the large contractions in the *c* axis direction.

Lithium diffusion in the Li layer occurs from one octahedral site to the adjacent octahedral site across a face-shared

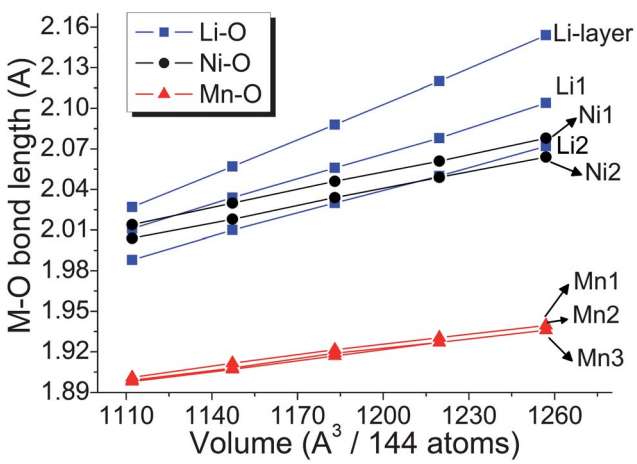

Fig. 3 Variation of the calculated Li–O and M–O bond lengths under pressure for $Li[Li_{1/6}Ni_{1/4}Mn_{7/12}]O_2$. The ordering in the TM layer is shown in Fig. 1.

This journal is © The Royal Society of Chemistry 2012

Downloaded by University of California - San Diego on 01 February 2012
Published on 01 February 2012 on http://pubs.rsc.org | doi:10.1039/C2EE02818B

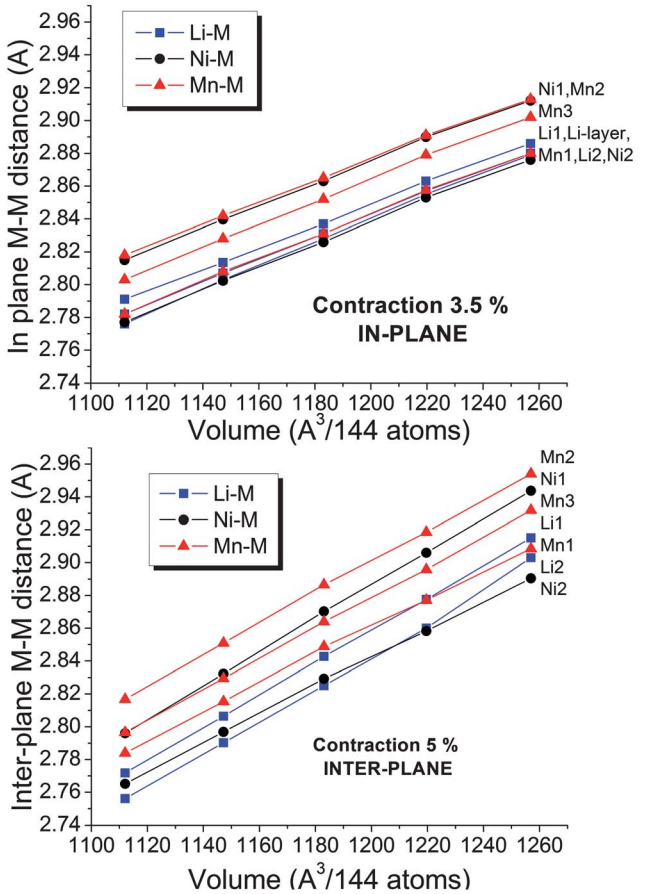

Fig. 4 Calculated in-plane (a) and inter-plane (b) contractions between adjacent metal ions in $Li[Li_{1/6}Ni_{1/4}Mn_{7/12}]O_2$ under pressure.

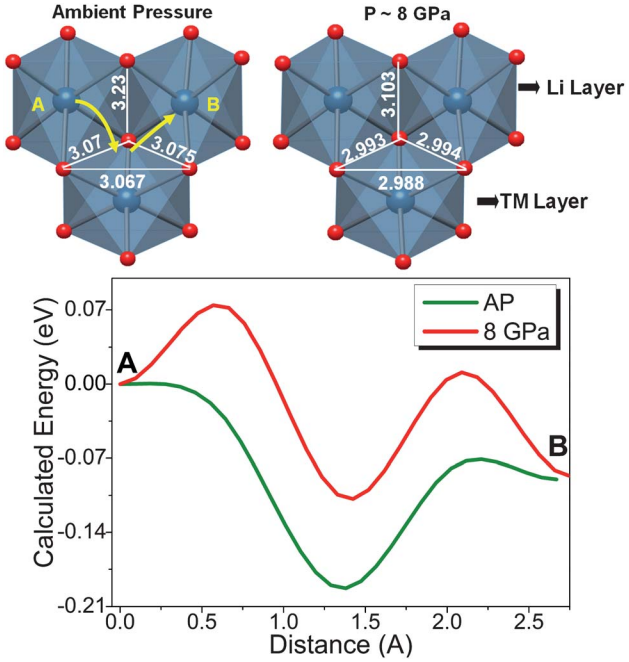

Fig. 5 (top) Sketch of the path for Li diffusion in the Li layer of $Li[Li_{1/6}Ni_{1/4}Mn_{7/12}]O_2$ at increasing pressures. Blue = Li and red = oxygen. The octahedral Li passes to the neighbour octahedral site across the adjacent tetrahedral site. (bottom) Calculated energy of the Li mobility at ambient pressure (green) and at *ca.* 8 GPa (red).

tetrahedral site, a path schematized in Fig. 5. During the hop, lithium ions can get trapped in the tetrahedral site forming a Li_{oct}–Li_{tet} dumbbell configuration with the Li ions in the adjacent TM layer. For $Li[Li_{1/6}Ni_{1/4}Mn_{7/12}]O_2$ previous investigations[26] have shown that the formation of such a configuration is favored during delithiation (at *ca.* 4.5 V). This originates structural transformation upon cycling causing the degradation of the electrode material. For the high pressure treated materials, one can expect that the more contracted oxygen arrangement precludes the mobility of Li ions from the octahedral sites into the tetrahedral sites, since the ions must cross a smaller triangular face, and occupy a smaller tetrahedral site. Fig. 5 compares the calculated energy path for Li motion in $Li_{5/6}[Li_{1/6}Ni_{1/4}Mn_{7/12}]O_2$ at ambient pressure and at a constant volume of 1183 $Å^3$, which corresponds to 8.0 GPa (see Fig. 2). According to previous works at ambient pressure, the Li ion will be trapped in the tetrahedral site, the stabilization energy being about 0.1 eV with respect to the more stable octahedral site. In the more contracted lattice, there is an energetic barrier of 0.07 eV to pass across the triangular face shared between octahedral and tetrahedral sites. Nevertheless the formation of tetrahedral lithium is still favored by 0.03 eV.

Based on the DFT results, some trends can be extracted. (i) The $Li[Li_{1/6}Ni_{1/4}Mn_{7/12}]O_2$ material is softer than $LiCoO_2$ or $LiNi_{0.5}Mn_{0.5}O_2$ and will undergo larger structural modifications under a HP/HT treatment. (ii) In layered $LiMO_2$, there is a notorious compression of the Li-layer. The TM ions have smaller ionic radii than Li and may easily be accommodated in the contracted Li layer; therefore, a high pressure treatment will favor a large Li–TM interlayer mixing. (iii) The more compact structure obtained upon HP/HT treatment will have lower ion mobility and hindered Li intercalation. (iv) During delithiation, the formation of tetrahedral Li is still energetically favored, though to a lesser extent.

Even though some predictions can be made, it is important to recall that high pressure materials are metastable phases at ambient pressure, and quite frequently quenched samples do not retain the crystal structure that is actually the thermodynamically stable form at high pressure. Obviously, the retention at ambient pressure of the stable high pressure-structure is also driven by kinetics. In short, the structural changes observed in quenched samples after a HP/HT treatment might be less severe than those anticipated from DFT.

3.2 Experimental results

3.2.1 $LiCoO_2$. Previous *in situ* high pressure experiments demonstrated that $LiCoO_2$ remains phase pure with the $R\bar{3}m$ space group up to 26 GPa and room temperature.[20] A compression of the unit cell of about 5% was observed, as discussed above related to the decreasing of the *c* lattice parameter and the high compressibility of the Li–O bonds. In the present work quenching experiments are performed, and therefore structural variations under pressure are not observed, but rather the resulting structural changes after a HP/HT treatment are reported.

X-Ray diffraction (XRD) patterns were collected from pristine and high pressure–high temperature treated $LiCoO_2$ (HP–$LiCoO_2$) at 4.0 GPa and 8.0 GPa at 1000 °C (see ESI†). Rietveld

Table 2 Rietveld refinement for pristine and high temperature high pressure treated $LiCoO_2$ and $Li[Ni_xLi_{1/3-2x/3}Mn_{2/3-x/3}]O_2$ ($x = 0.5, 0.25$). n_TM (Co, Ni) is the occupation of the 3*b* site (Li layer) by nickel or cobalt with the remainder of atoms on the site being lithium

	Pristine	5.2 Gpa	8.0 Gpa
$LiCoO_2$	$a = 2.8155$ $c = 14.0473$ $c/a = 4.989$ $V = 96.43$ $z(O) = 0.2577$ n_Co = 0.001 $R_{wp} = 4.83$; $R_b = 5.62$	$a = 2.8127$ $c = 14.0441$ $c/a = 4.993$ $V = 96.22$ $z(O) = 0.2597$ n_Co = 0.061 $R_{wp} = 4.97$; $R_b = 3.77$	$a = 2.8120$ $c = 14.0406$ $c/a = 4.993$ $V = 96.15$ $z(O) = 0.2600$ n_Co = 0.007 $R_{wp} = 3.54$; $R_b = 6.62$
$LiNi_{0.5}Mn_{0.5}O_2$	$a = 2.8900$ $c = 14.2975$ $c/a = 4.947$ $V = 103.42$ $z(O) = 0.2563$ n_Ni = 0.117 $R_{wp} = 5.03$; $R_b = 3.01$	$a = 2.8975$ $c = 14.2908$ $c/a = 4.932$ $V = 103.90$ $z(O) = 0.2559$ n_Ni = 0.197 $R_{wp} = 3.56$; $R_b = 4.77$	$a = 2.9165$ $c = 14.2914$ $c/a = 4.900$ $V = 105.276$ $z(O) = 0.2561$ n_Ni = 0.322 $R_{wp} = 5.65$; $R_b = 12.1$
$Li[Li_{1/6}Ni_{1/4}Mn_{7/12}]O_2$	$a = 2.8667$ $c = 14.2772$ $c/a = 4.980$ $V = 101.61$ $z(O) = 0.2580$ n_Ni = 0.039 $R_{wp} = 14.5$; $R_b = 7.6$	***Phase 1:*** $a = 2.8600$ $c = 14.2380$ $c/a = 4.978$ $V = 100.86$ $z(O) = 0.2570$ n_Ni = 0.047 Phase fraction: 67% ***Phase 2:*** $a = 2.9022$ $c = 14.2887$ $c/a = 4.923$ $V = 104.23$ $z(O) = 0.2580$ n_Ni = 0.164 $R_{wp} = 7.92$; $R_b = 4.03$	

refinements of the patterns indicate that the post-treated materials remain phase pure. Table 2 shows the Rietveld refinement results following HP/HT treatment. The *c* lattice parameters decrease less than 1% from 14.047 Å to 14.040 Å while the *a* lattice parameters decrease from 2.816 Å to 2.812 Å resulting in a 0.3% decrease in cell volume as the pressure increases. The findings confirm that HP/HT (up to 8 GPa/1000 °C) does not drastically affect $LiCoO_2$, as it was observed during *in situ* experiments. Fig. 6 compares the electrochemical cycling profile of pristine $LiCoO_2$ and the post-treated $LiCoO_2$. The two post-treated materials are electrochemically active showing capacities

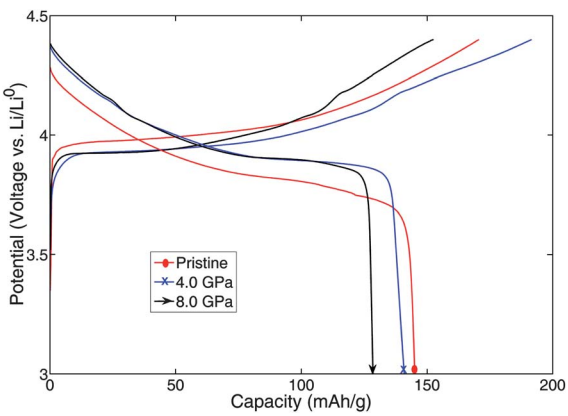

Fig. 6 Comparison of the electrochemical cycling profile of pristine $LiCoO_2$ (red) and high pressure treated $LiCoO_2$ at 4.0 GPa (blue X) and 8.0 GPa (black arrow). A voltage window of 4.4–3.0 V was used.

and voltage profile very similar to the pristine material. High pressure and high temperature treatment to 8.0 GPa and 1000 °C does not significantly affect the electrochemical properties.

3.2.2 $LiNi_{0.5}Mn_{0.5}O_2$ ($x = 0.5$). Fig. 7 shows the XRD patterns collected from $LiNi_{0.5}Mn_{0.5}O_2$ as synthesized (Fig. 7a) and following high pressure/high temperature treatment at 8.0 GPa (Fig. 7b). The pattern of the sample treated at 5.2 GPa is shown in the ESI†. Examining the XRD patterns of the post-treated samples indicates that an unknown secondary phase may have formed as evidenced by shoulders on the high 2θ side of the (104) peak; however, fitting using the $Fd\bar{3}m$ or $C2/m$ space groups for this second phase did not yield acceptable results. The results of fitting the sample to the $R\bar{3}m$ space group can be seen in Table 2. As the pressure increases to 8.0 GPa, the *c*/*a* lattice ratio decreases from 4.947 to 4.900. Moreover, the amount of Li/Ni mixing increases from 11% to 32% following treatment at 8.0 GPa. The intensity ratio of the (003) peak *versus* the (104) peak is an indicator of the layeredness of the material.[28] The $I(003)/I(004)$ ratio decreases from 0.78 in the pristine sample to 0.43 at 5.2 GPa to 0.18 in the 8.0 GPa sample. Moreover, the intensity ratio of the (101) to ((006) + (012)) peaks decreases, and the degree of peak separation (110)/(018) doublet shrinks indicating that the layeredness of the material worsens.[28–30] These findings are in good agreement with DFT results.

The structural modifications observed in the X-ray diffraction profiles are confirmed in the electrochemical testing. It is well established that for $LiNi_{0.5}Mn_{0.5}O_2$, a larger amount of Li/Ni mixing is detrimental to the electrochemical performance.[31]

Downloaded by University of California - San Diego on 01 February 2012
Published on 01 February 2012 on http://pubs.rsc.org | doi:10.1039/C2EE02818B

 This journal is © The Royal Society of Chemistry 2012

Downloaded by University of California - San Diego on 01 February 2012
Published on 01 February 2012 on http://pubs.rsc.org | doi:10.1039/C2EE02818B

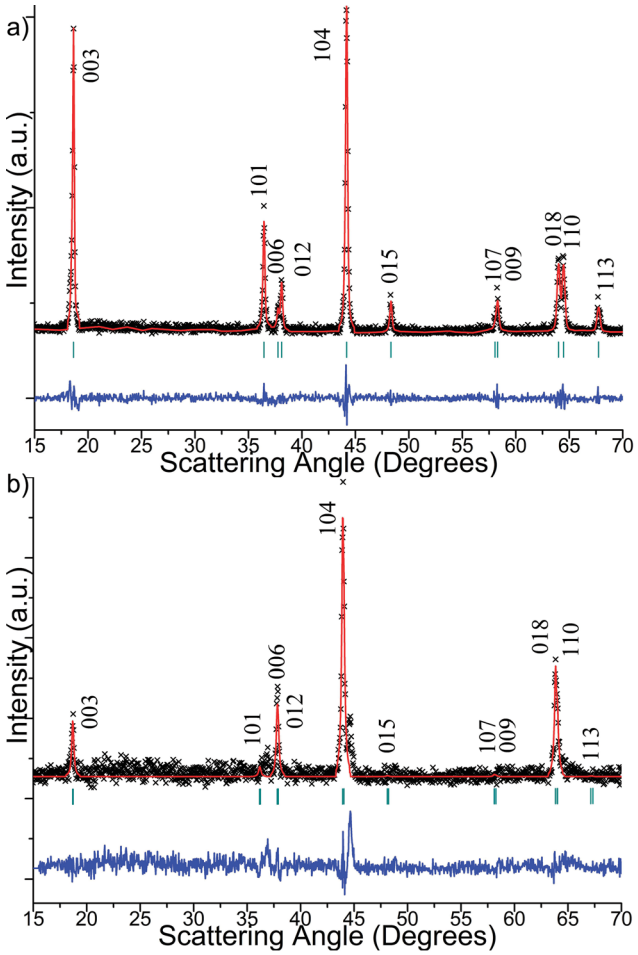

Fig. 7 The Rietveld refinement results from XRD patterns collected from $LiNi_{0.5}Mn_{0.5}O_2$ (a) as synthesized and following high pressure/high temperature treatment at (b) 8.0 GPa at 1000 °C.

Accordingly, increasing HP/HT treatment increases the Li/Ni mixing and consequently inhibits the electrochemical performance. Fig. 8 shows the first cycle charge and discharge profiles. The pristine material yields charge and discharge capacities of 189 mA h g^{-1} and 164 mA h g^{-1}, respectively, within the 4.8–2.0 V voltage window. Following HP/HT treatment, the sample treated at 5.2 GPa yields 140 mA h g^{-1} upon charging; however only 80 mA h g^{-1} is reversible following the first discharge. The capacity further fades when the material is treated at 8.0 GPa, with initial charge and discharge capacities of 69 mA h g^{-1} and 23 mA h g^{-1} respectively.

3.2.3 Lithium excess $Li[Li_{1/6}Ni_{1/4}Mn_{7/12}]O_2$ (x = 0.25). Fig. 9a shows the synchrotron X-ray diffraction pattern of the pristine $Li[Li_{1/6}Ni_{1/4}Mn_{7/12}]O_2$. The pristine phase can be indexed to the typical $R\bar{3}m$ phase and shows good layering with 4% Li/Ni mixing. Fig. 9b illustrates that the X-ray diffraction pattern of the HP/HT materials exposed to 5.2 GPa still shows the superlattice peaks between 20 and 30° observed in the pristine materials, which are associated with a honeycomb ordering of Li^+, Ni^{2+} and Mn^{4+} in the transition metal layer consistent with the Li_2MnO_3-end member type ordering.[32,33] The XRD pattern of the post-treated material shows distinct evidence of second

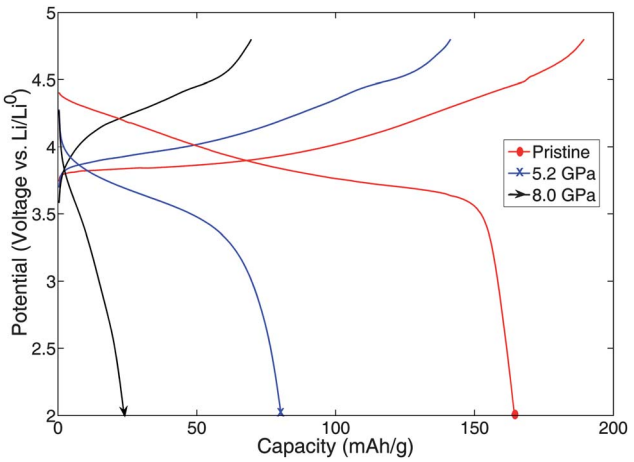

Fig. 8 Comparison of the electrochemical cycling profile of pristine $LiNi_{0.5}Mn_{0.5}O_2$ (red) and HP/HT treated $LiNi_{0.5}Mn_{0.5}O_2$ at 5.2 GPa (blue X) and 8.0 GPa (black arrow). A voltage window of 4.8–2.0 V was used.

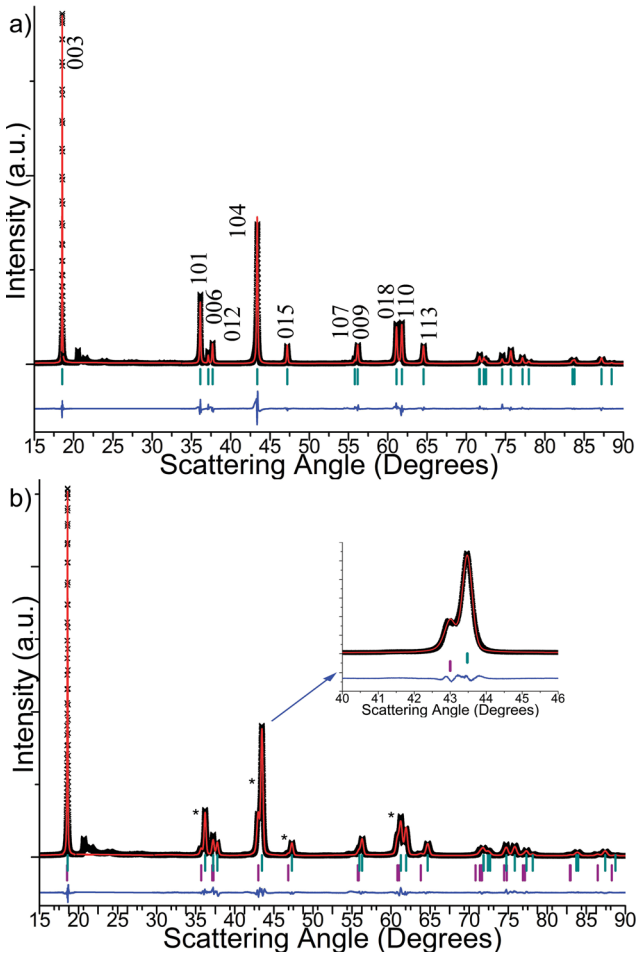

Fig. 9 A comparison of the Rietveld refinement results from X-ray diffraction (XRD) patterns collected from (a) pristine $Li[Li_{1/6}Ni_{1/4}Mn_{7/12}]O_2$ and exposed to HP/HT treatments at (b) 5.2 GPa. The second phase is represented with (*). The 2θ region between 20 and 30° excluded from fitting results.

Downloaded by University of California - San Diego on 01 February 2012
Published on 01 February 2012 on http://pubs.rsc.org | doi:10.1039/C2EE02818B

phase formation in addition to the superlattice peaks as evidenced by additional peak/shoulders next to the (101), (104), (018) and (110) peaks. The XRD pattern collected following HPHT treatment at 8.0 GPa shows that the secondary peak intensities increased (see ESI†). From a structural viewpoint, the Rietveld refinement results, seen in Table 2, indicate that at 5.2 GPa, two layered phases exist. The primary phase shows a 0.07 Å and a 0.04 Å decrease in the *a* and *c* lattice parameters respectively, indicating a densification of the primary phase. The calculations predicted stronger out-of-plane lattice contractions of the material which is observed in the refinement of the XRD pattern. The amount of Li/Ni mixing remains similar below 5%. In the secondary phase, the amount of Li/Ni mixing increases to 16%. Also the *a* and *c* lattice parameters increase 0.035 Å and 0.012 Å from the pristine material respectively, causing the *c*/*a* ratio to decrease which is an indication of decreased layeredness.[28]

Fig. 10 compares the electrochemical properties during the first charge/discharge cycle of the pristine lithium excess material and following high pressure treatment at 5.2 GPa and 8.0 GPa. The HP/HT treated samples display a good electrochemical response, unlike the case of $LiNi_{0.5}Mn_{0.5}O_2$. The HPHT treated samples have the same absolute irreversible capacity, but a lower reversible capacity than the untreated material indicating that the treatment does not improve the first cycle capacity loss. Both materials exposed to high pressure and high temperature showed initial charge capacities exceeding 200 mA h g^{-1}. There are important differences, particularly in the plateau region of 4.5 V which corresponds to the oxygen removal or surface modification reactions. It has been shown that these charge compensation mechanisms are accompanied with simultaneous oxygen removal or activation.[8,10,34] The decreasing voltage plateau length shows that not only does the anomalous capacity originate through the activation of oxygen but concurrently is the charge compensated through transition metal migration, Li^+ ion tetrahedral formation and second layered phase formation. The pristine material displayed the longest plateau region as well as a lower voltage during charging than the HP/HT materials. As the level of pressure applied to the material increased, the length of the plateau region at 4.5 V decreased with the associated specific capacity decreasing from 110 mA h g^{-1} (pristine) to 85 mA h g^{-1} (5.2 GPa) to 20 mA h g^{-1} (8.0 GPa). As the plateau region shortens, the amount of structural rearrangement would be expected to be reduced; however, we observe the same extent of structural rearrangement following electrochemical cycling as in the pristine material. Fig. 11 shows the capacity retention with cycling for pristine and the material treated at 5.2 GPa. Both materials are able to show reversible capacities exceeding 200 mA h g^{-1} after the first discharge and stable charge and discharge capacities for the first 10 cycles.

Following ten electrochemical cycles, the cathode material exposed to HP/HT treatment at 5.2 GPa was recovered. Fig. 12 shows the collected X-ray diffraction pattern. This pattern can be compared with the pristine material following electrochemical cycling shown in ref. 26. Important changes are observed compared with the initial HP/HT material (Fig. 9b). Both the superlattice peaks and the evidence of distinct shoulders have drastically decreased in intensity or disappeared. The disappearance of the superlattice peaks was previously observed for

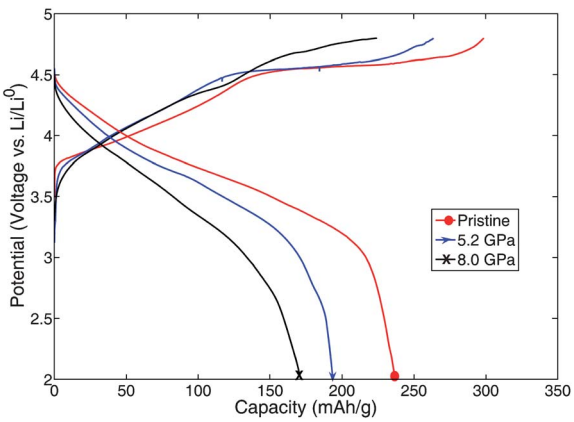

Fig. 10 First cycle electrochemical profiles of pristine $Li[Li_{1/6}Ni_{1/4}Mn_{7/12}]O_2$ (red) and those exposed to HP/HT treatments at 5.2 GPa (blue arrow) and 8.0 GPa (black X) and 1000 °C. Voltage windows of 4.8–2.0 V were used.

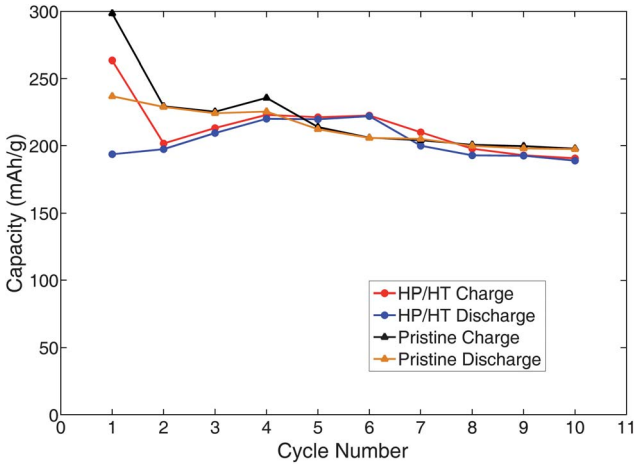

Fig. 11 Comparison of the cycling stability of $Li[Ni_{1/4}Li_{1/6}Mn_{7/12}]O_2$ before and after HP/HT treatment at 5.2 GPa.

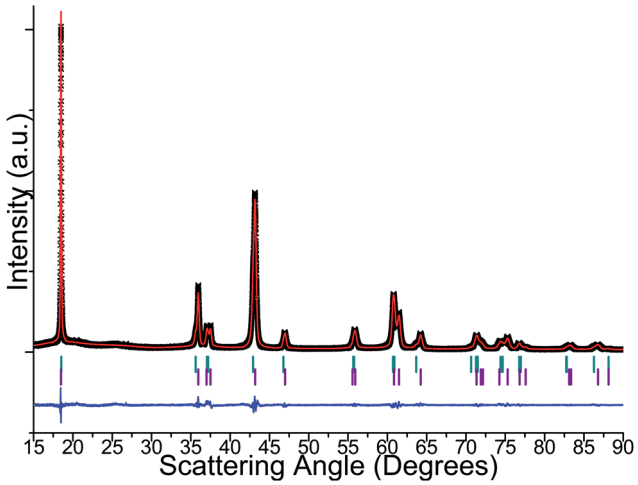

Fig. 12 Rietveld refinement results from X-ray diffraction (XRD) patterns collected from $Li[Li_{1/6}Ni_{1/4}Mn_{7/12}]O_2$ exposed to HP/HT treatments at 5.2 GPa following 10 electrochemical cycles.

 This journal is © The Royal Society of Chemistry 2012

Downloaded by University of California - San Diego on 01 February 2012
Published on 01 February 2012 on http://pubs.rsc.org | doi:10.1039/C2EE02818B

the pristine material and it was ascribed to the loss of cation ordering in the TM layer.[4,26] In Fig. 12, the Rietveld refinement of the XRD pattern following electrochemical cycling using two layered phases led to improved fitting parameters. As predicted by DFT results, the introduction of tetrahedral lithium into the secondary phase further improved the fitting parameters as seen in Table 3. The Rietveld refinement indicates that following electrochemical cycling, both phases expand and TM ions migrate to and from the Li layer. The amount of Li/Ni mixing increases from 0.047 to 0.066 in the primary phase and decreases from 0.164 to 0.150 in the secondary phase. This indicates that during electrochemical cycling the material undergoes large changes in cation occupancies, lattice parameters, as well as formation of a secondary phase with tetrahedral Li, yet remains electrochemically active displaying large specific capacities. The details of the cation migrations and structural changes have been reported in our previous paper.[26]

4. Discussion

In this work, we aimed to induce structural modifications in the layered materials by HP/HT treatment in order to get a better understanding of the electrochemical behavior dependence with structural factors. This knowledge is critical for the commercialization and application of the promising Li-excess electrode materials. HP/HT techniques provided a unique way of introducing structural modifications in the layered materials. We have shown that the structural modifications that can be achieved following a HP/HT treatment are different from those attainable by altering other variables in the synthesis process, such as the nature of the reactants or the temperature of synthesis.

The results obtained for $LiCoO_2$, $LiNi_{0.5}Mn_{0.5}O_2$ and $Li[Li_{1/6}Ni_{1/4}Mn_{7/12}]O_2$ following HP/HT treatment reveal that these layered materials display a large resistance to structure collapse or phase transformation. It should be noted that samples have been subjected to pressures up to 8 GPa at 1000 °C. Under similar conditions other electrode materials have already transformed to high-pressure polymorphs, or decomposed. Indeed the calculated bulk moduli (around 130 GPa) of these layered oxides are larger than those of most electrode materials; V_2O_5 (calculated 20 GPa[35]), Li_2MSiO_4 (M=Co, Mn; experimental 90 GPa[36]), $LiCoPO_4$ (calculated 80 GPa[37]), and $FePO_4$ (experimental 24 GPa[38]). Within the family of layered materials $Li[Li_xM_{1-x}]O_2$, the compressibility is a function of the nature of TM and the Li content. DFT calculations clearly showed that Li–O bonds are twice as compressible as M–O bonds. Furthermore, the substitution of Co with Li, Ni and Mn in the transition metal layer softens the material and decreases the bulk modulus. Rietveld refinement of the XRD spectra following high pressure treatment confirms these results. $LiCoO_2$ showed minimal structural changes. Conversely, $LiNi_{0.5}Mn_{0.5}O_2$ and $Li[Li_{1/6}Ni_{1/4}Mn_{7/12}]O_2$ showed large structural changes and in the latter the formation of a second layered phase is observed.

Synthetic history and consequent structural modifications impose a fingerprint in the electrochemical behavior. The electrochemical properties of both high pressure treated $LiCoO_2$ samples were nearly identical to the pristine material, as expected for the minor structural distortion observed. The high pressure treatment of $LiNi_{0.5}Mn_{0.5}O_2$ ($x = 0.5$) caused considerable structural modifications that decreased the layered characteristics of the material and increased the amount of Li/Ni mixing. As the Li–O bonds are twice as compressible compared to M–O bonds, the effect of pressure is to equalize the thickness of TM and Li layers favoring interlayer mixing. The electrochemical properties of $LiNi_{0.5}Mn_{0.5}O_2$ are optimal with minimal Li/Ni interlayer mixing. The first electrochemical cycle indicates that as the pressure of the treatment increases, the material becomes less electrochemically active. It is likely that the increased structural disorder from the Li/Ni mixing may have blocked the Li intercalation pathways inhibiting the electrochemical performance of the material. Besides blocking of the Li paths by interlayer mixing, we have shown that densification of the lattice under pressure may also hinder the Li mobility (Fig. 5). In the end, the structural modifications induced by the HP/HT treatment turn the samples electrochemically inactive.

The Li excess material has increased amounts of Li–O bonding originating from Li in the transition metal layer. This bonding shows the largest calculated compressibility and first principles calculations anticipated major structural changes for the lithium excess $Li[Li_{1/6}Ni_{1/4}Mn_{7/12}]O_2$ material. Indeed the analysis of the X-ray diffraction data indicates that the material forms a second layered phase. This phase shows an expanded lattice as well as a 0.125 increase in Li/Ni mixing compared to the pristine material. The primary phase shows 0.04 Å reduction in the c lattice parameter from the pristine structure. The amount of Li/Ni mixing remains nearly 4% following the treatment. Surprisingly, and in contrast to what happened with $LiNi_{0.5}Mn_{0.5}O_2$, all these structural rearrangements do not result in a deterioration of the electrochemical behavior. The material was able to display electrochemical capacities exceeding 200 mA h g^{-1} for 10 cycles.

Interestingly, the anomalous capacities of the high pressure material resulted in a shorter plateau region at 4.5 V. It has been shown that the source of excess Li and the plateau region is related to the activation of Li_2MnO_3 (or $Li[Li_{1/3}Mn_{2/3}]O_2$) *via*

Table 3 Rietveld refinement results for $Li[Ni_xLi_{1/3-2x/3}Mn_{2/3-x/3}]O_2$ ($x = 0.25$) following 5.2 GPa treatment and 10 electrochemical cycles. n_Ni is the occupation of the 3*b* site (Li layer) by nickel with the remainder of atoms on the site being lithium. n_Li is the occupation of the tetrahedral site by lithium (1/3, 2/3, $z = 0.810$)

	Pristine after 5.2 GPa	Following 10 electrochemical cycles
$Li[Li_{1/6}Ni_{1/4}Mn_{7/12}]O_2$ following HP/HT treatment at 5.2 GPa	***Phase 1:***	***Phase 1:***
	$a = 2.8600$	$a = 2.8814$
	$c = 14.2380$	$c = 14.3381$
	$c/a = 4.978$	$c/a = 5.006$
	$z(O) = 0.2570$	$z(O) = 0.2570$
	n_Ni = 0.047	n_Ni = 0.066
	Phase fraction: 67%	Phase fraction: 60%
	Phase 2:	***Phase 2:***
	$a = 2.9022$	$a = 2.9095$
	$c = 14.2887$	$c = 14.3118$
	$c/a = 4.923$	$c/a = 5.004$
	$z(O) = 0.2580$	$z(O) = 0.2580$
	n_Ni = 0.164	n_Ni = 0.15, n_Li = 0.14
	$R_{wp} = 7.92$; $R_b = 4.03$	$R_{wp} = 5.7$; $R_b = 2.33$

Downloaded by University of California - San Diego on 01 February 2012
Published on 01 February 2012 on http://pubs.rsc.org | doi:10.1039/C2EE02818B

oxygen loss.[6,10] Based on X-ray diffraction and the electrochemical results, we predict that the second layered phase that forms following HP/HT treatment may be related to the $Li[Li_{1/3}Mn_{2/3}]O_2$-type end member of $Li[Ni_xLi_{1/3-2x/3}Mn_{2/3-x/3}]O_2$ with large amounts of defects. The structure obtained from Rietveld refinement of the secondary layered phase could be written as $Li_{0.84}Ni_{0.16}[Li_{1/3}Mn_{7/12}Ni_{1/12}]O_2$, within experimental error, which is structurally equivalent to $Li[Li_{1/3}TM_{2/3}]O_2$. This phase is believed to account for the majority of the anomalous capacity observed during the voltage plateau region.[11,39] Following electrochemical cycling of the Li excess material, the shoulders at the majority of the peaks seen in the uncycled 5.2 GPa treated sample disappear and decrease in intensity. Also, the amount of structural reorganization including lattice expansion and cation migration is large as seen in Table 3. Rietveld refinement indicates that tetrahedral Li occupancy may be observed following electrochemical cycling of the high pressure material. DFT data predicted that the formation of tetrahedral Li is still energetically favorable in the compressed lattice. Additionally, the material still exists as two layered phases, with one phase including tetrahedral Li. Similarly as previously studied, the lattices of both phases expand and the amount of Li/Ni mixing increases compared to that of the pristine untreated sample.[26] The electrochemical results show that as the pressure increases, the length of the plateau region decreases indicating that the amount of Li_2MnO_3 activation is decreased, which may be due to the phase separation of the two end members that form the solid solution of $Li[Ni_xLi_{1/3-2x/3}Mn_{2/3-x/3}]O_2$.

The results reported indicate that significant structural rearrangement occurs in the HPHT treated Li-excess layered material during electrochemical cycling. It is expected that the formation of a second layered phase and increased cation mixing induced by HPHT treatment before cycling would hinder the electrochemical characteristics of the Li-excess material. However, the material structurally rearranges during electrochemical cycling to improve the layered characteristics unlike $LiNi_{0.5}Mn_{0.5}O_2$. The results identified here indicate that the structural rearrangements seen during the first electrochemical cycle are critical for the electrochemical activation of the material. Further research identifying when and how structural modifications occur during the first electrochemical cycle are necessary to understand how to improve the intrinsically poor rate capability and irreversible capacity loss.

5. Conclusions

Efforts to improve the performance of layered $LiMO_2$ cathode materials involve a deep understanding of the connection between crystal structure and electrochemical properties. In this context, we have investigated the high pressure-treated layered materials $LiCoO_2$ and $Li[Ni_xLi_{1/3-2x/3}Mn_{2/3-x/3}]O_2$ where $x = 0.25$ and 0.5 combining both computational and experimental methods. We can conclude that the substitution of Co for Ni and Mn softens the layered oxides and the introduction of Li in the transition metal layer further softens the material. Some of the structural modifications induced by the HP/HT treatment are retained in the quenched samples, resulting in electrode characteristics different from those of the pristine materials.

For $LiCoO_2$, the minor structural modifications have nearly no impact in the electrochemistry. In $LiNi_{0.5}Mn_{0.5}O_2$ following the high pressure treatment, there is an increasing interlayer mixing which causes poor electrochemical activity. The Li excess material suffers the more drastic structural modifications following HP/HT treatment. However the post-treated samples display a good electrochemical response. Structural modifications have also been observed during the cycling of the high-pressure treated samples. Regardless of these structural modifications the material can reversibly cycle at capacities near that obtained from the as-synthesized material. These results indicate that the lithium excess layered material has the ability of undergoing large compressions and structural modifications while delivering electrochemical capacities exceeding 200 mA h g^{-1}. In that sense, the Li excess materials are superior to $LiNi_{0.5}Mn_{0.5}O_2$, whose electrochemical characteristics are very sensitive to structural modifications.

Acknowledgements

M.E. Arroyo-de Dompablo acknowledges financial support from the Spanish Ministry of Science (MAT2007-62929, CSD2007-00045) and the project S2009-PPQ/1551 funded by Comunidad Autónoma de Madrid. Y. S. Meng and D. H. Lee would like to express the gratitude to University of California San Diego for the new faculty startup funding. C. R. Fell acknowledges the financial support from Florida Energy System Consortium through University of Florida under award number 80859. The synchrotron X-ray diffraction patterns were collected at Argonne National Laboratory on beamline 11-BM through the general user proposal mail-in program (GUP-13210). The authors would like to thank Ms Bo Xu, Ms Danna Qian and Mr M. Yang for their valuable discussions. M.E. Arroyo-de Dompablo is grateful to Ms M. Ruiz Santa Quiteria for assistance in the analysis of the computational data.

References

1 J. Reed and G. Ceder, *Electrochem. Solid-State Lett.*, 2002, **5**, A145–A148.
2 W. S. Yoon, S. Iannopollo, C. P. Grey, D. Carlier, J. Gorman, J. Reed and G. Ceder, *Electrochem. Solid-State Lett.*, 2004, **7**, A167–A171.
3 T. Ohzuku and Y. Makimura, *Chem. Lett.*, 2001, 744–745.
4 Y. S. Meng, G. Ceder, C. P. Grey, W. S. Yoon, M. Jiang, J. Breger and Y. Shao-Horn, *Chem. Mater.*, 2005, **17**, 2386–2394.
5 R. D. Shannon and C. T. Prewitt, *Acta Crystallogr., Sect. B: Struct. Crystallogr. Cryst. Chem.*, 1969, **B25**, 925.
6 M. M. Thackeray, S.-H. Kang, C. S. Johnson, J. T. Vaughey, R. Benedek and S. A. Hackney, *J. Mater. Chem.*, 2007, **17**, 3112–3125.
7 M. Jiang, B. Key, Y. S. Meng and C. P. Grey, *Chem. Mater.*, 2009, **21**, 2733–2745.
8 Z. Lu and J. R. Dahn, *J. Electrochem. Soc.*, 2002, **149**, A815–A822.
9 D. D. MacNeil, Z. Lu and J. R. Dahn, *J. Electrochem. Soc.*, 2002, **149**, A1332–A1336.
10 A. R. Armstrong, M. Holzapfel, P. Novak, C. S. Johnson, S. H. Kang, M. M. Thackeray and P. G. Bruce, *J. Am. Chem. Soc.*, 2006, **128**, 8694–8698.
11 A. D. Robertson and P. G. Bruce, *Electrochem. Solid-State Lett.*, 2004, **7**, A294–A298.
12 C. R. Fell, K. J. Carroll, M. Chi and Y. S. Meng, *J. Electrochem. Soc.*, 2010, **157**, A1202–A1211.
13 R. A. Binns, R. J. Davis and S. J. B. Reed, *Nature*, 1969, **221**, 943–944.
14 M. E. Arroyo-de Dompablo, J. M. Gallardo-Amores and U. Amador, *Electrochem. Solid-State Lett.*, 2005, **8**, A564–A569.

 This journal is © The Royal Society of Chemistry 2012

15 M. E. Arroyo y de Dompablo, U. Amador, J. M. Gallardo-Amores, E. Morán, H. Ehrenberg, L. Dupont and R. Dominko, *J. Power Sources*, 2009, **189**, 638–642.
16 O. García-Moreno, M. Alvarez-Vega, J. García-Jaca, J. M. Gallardo-Amores, M. L. Sanjuán and U. Amador, *Chem. Mater.*, 2001, **13**, 1570–1576.
17 M. E. Arroyo y de Dompablo, J. M. Gallardo-Amores, U. Amador and E. Morán, *Electrochem. Commun.*, 2007, **9**, 1305–1310.
18 R. Stoyanova, E. Zhecheva, R. Alcantara, J.-L. Tirado, G. Bromiley, F. Bromiley and T. B. Ballaran, *J. Mater. Chem.*, 2004, **14**, 366–373.
19 R. Stoyanova, E. Zhecheva, R. Alcántara, J. L. Tirado, G. Bromiley, F. Bromiley and T. Boffa Ballaran, *Solid State Ionics*, 2003, **161**, 197–204.
20 X. Wang, I. Loa, K. Kunc, K. Syassen and M. Amboage, *Phys. Rev. B: Condens. Matter Mater. Phys.*, 2005, **72**, 224102.
21 M. Yoncheva, R. Stoyanova, E. Zhecheva, R. Alcantara, G. Ortiz and J. L. Tirado, *J. Solid State Chem.*, 2007, **180**, 1816–1825.
22 G. Kresse and J. Hafner, *Phys. Rev. B: Condens. Matter Mater. Phys.*, 1994, **49**, 14251.
23 G. Kresse and J. Furthmüller, *Comput. Mater. Sci.*, 1996, **6**, 15–50.
24 G. Kresse and J. Furthmüller, *Phys. Rev. B: Condens. Matter Mater. Phys.*, 1996, **54**, 11169.
25 A. Van der Ven and G. Ceder, *Electrochem. Commun.*, 2004, **6**, 1045–1050.
26 B. Xu, C. R. Fell, M. Chi and Y. S. Meng, *Energy Environ. Sci.*, 2011, **4**, 2223.
27 F. D. Murnaghan, *Proc. Natl. Acad. Sci. U. S. A.*, 1944, **30**, 244.
28 R. J. Gummow, M. M. Thackeray, W. I. F. David and S. Hull, *Mater. Res. Bull.*, 1992, **27**, 327–337.
29 E. Rossen, C. D. W. Jones and J. R. Dahn, *Solid State Ionics*, 1992, **57**, 311–318.
30 R. Stoyanova, E. Zhecheva and L. Zarkova, *Solid State Ionics*, 1994, **73**, 233–240.
31 K. S. Kang, Y. S. Meng, J. Breger, C. P. Grey and G. Ceder, *Science*, 2006, **311**, 977–980.
32 P. Strobel and B. Lambert-Andron, *J. Solid State Chem.*, 1988, **75**, 90–98.
33 V. Massarotti, M. Bini, D. Capsoni, A. Altomare and A. G. G. Moliterni, *J. Appl. Crystallogr.*, 1997, **30**, 123–127.
34 N. Yabuuchi, K. Yoshii, S.-T. Myung, I. Nakai and S. Komaba, *J. Am. Chem. Soc.*, 2011, **133**, 4404–4419.
35 J. M. Gallardo-Amores, N. Biskup, U. Amador, K. Persson, G. Ceder, E. Morán and M. E. Arroyo y de Dompablo, *Chem. Mater.*, 2007, **19**, 5262–5271.
36 D. Santamaría-Pérez, U. Amador, J. Tortajada, R. Dominko and M. E. Arroyo-de Dompablo, in preparation.
37 U. Amador, J. M. Gallardo-Amores, G. Heymann, H. Huppertz, E. Moran and M. E. Arroyo-de Dompablo, *Solid State Sci.*, 2008, **11**, 343–348.
38 M. P. Pasternak, G. K. Rozenberg, A. P. Milner, M. Amanowicz, T. Zhou, U. Schwarz, K. Syassen, R. Dean Taylor, M. Hanfland and K. Brister, *Phys. Rev. Lett.*, 1997, **79**(22), 4409–4412.
39 A. D. Robertson and P. G. Bruce, *Chem. Mater.*, 2003, **15**, 1984–1992.

Downloaded by University of California - San Diego on 01 February 2012
Published on 01 February 2012 on http://pubs.rsc.org | doi:10.1039/C2EE02818B